

The influence of magnetic field on RM instability of circular heavy gas eruption

Zhenya Lin, Zhihua Chen, Ying Liu

Key Laboratory of Transient Physics, Nanjing University of Science and Technology
Nanjing 210094, Jiangsu Province, China

1 Introduction

The hydrodynamic instabilities induced by the explosion of high pressure gas cloud include Rayleigh-Taylor (RT) instability, Richtmyer-Meshkov (RM) and Kelvin-Helmholtz (KH). Massive numerical simulation and experiments show that, hydrodynamic instability has become the key factor that restricts the success of inertial confinement fusion. Therefore, Suppressing such instabilities are important.

The quantitative understanding of the RM instability has been a grand challenge to the computational fluid dynamics (CFD). In 1995, Holmes et al. [1] published their results of numerical simulations of two RM instability experiments, Benjamin's air-SF6 and Meshkov's air-He experiments, using the front-tracking method developed by Chern et al. [2] and Glimm et al. [3-4]. Holmes et al. [1] pointed out that the growth rate of the shocked interface would decelerate, which is caused by the effects of the reshock produced by the self-interactions of the transmitted and reflected waves at the boundary walls. They proved it by providing the pressure plots of their simulations at some critical times to capture this nonlinear and compressive phenomenon. Recently, several numerical simulations of RM instabilities also showed improved agreement with experiments (see [5-7]).

MHD techniques have been applied to control the hypersonic flow. In this paper, we investigate numerically to use MHD suppressing the RM instability caused by the high pressure heavy gas eruption.

2 Governing Equations

The MHD equations are given as

$$\frac{\partial \rho}{\partial t} + \nabla \cdot [\rho \mathbf{v}] = 0 \quad (1)$$

$$\frac{\partial (\rho \mathbf{v})}{\partial t} + \nabla \cdot \left[\rho \mathbf{v} \mathbf{v} - \frac{\mathbf{B} \mathbf{B}}{\mu} + P^* \right] = -\nabla \cdot \mathbf{\Pi} \quad (2)$$

$$\frac{\partial E}{\partial t} + \nabla \cdot \left[(E + P^*) \mathbf{v} - \frac{\mathbf{B} (\mathbf{B} \cdot \mathbf{v})}{\mu} \right] = -\nabla \cdot \mathbf{Q} - \nabla \cdot (\mathbf{\Pi} \cdot \mathbf{v}) \quad (3)$$

$$\frac{\partial \mathbf{B}}{\partial t} - \nabla \times (\mathbf{v} \times \mathbf{B}) = 0 \quad (4)$$

where

$$P^* = P + \frac{\mathbf{B} \cdot \mathbf{B}}{2\mu}, \quad E = P / (\gamma - 1) + \frac{\rho(\mathbf{v} \cdot \mathbf{v})}{2} + \frac{\mathbf{B} \cdot \mathbf{B}}{2\mu}, \quad \mathbf{J} = \frac{1}{\mu} \nabla \times \mathbf{B}$$

$$\mathbf{Q} = -\kappa_0 \nabla T - \kappa_{\parallel} \hat{\mathbf{b}} \hat{\mathbf{b}} \cdot \nabla T, \quad \mathbf{\Pi} = -v_0 \nabla \mathbf{v} - 3v_{\parallel} \left(\hat{\mathbf{b}} \hat{\mathbf{b}} - \frac{1}{3} \mathbf{I} \right) \left(\hat{\mathbf{b}} \hat{\mathbf{b}} - \frac{1}{3} \mathbf{I} \right) : \nabla \mathbf{v}$$

$\mathbf{\Pi}$ is the viscous stress tensor, which contains both isotropic and anisotropic components, controlled by the coefficients v_0 and v_{\parallel} respectively. In the anisotropic case, the viscous flux is confined to be parallel to the magnetic field lines.

\mathbf{Q} is the heat flux, which contains both isotropic and anisotropic components, controlled by the coefficients κ_0 and κ_{\parallel} respectively. In the anisotropic case, the heat flux is confined to be parallel to the magnetic field lines.

3 Numerical Methods

The corner transport upwind (CTU) algorithm is an unsplit, 2D finite volume algorithm for solving hyperbolic systems of conservation laws, and the constrained transport (CT) algorithm is applied to preserve the divergence-free constraint on the magnetic field [9]. To make this point more concrete, the parallel flux gradient terms (x-flux gradient at x-interfaces, etc.) are included in the PPM interface states algorithm using the dimensionally split method. Meanwhile, the transverse flux gradient terms are included using the conservative form of the equations. Since the dimensionally split primitive and conservative form of the equations for MHD are not commensurate. In addition, such an algorithm would also show secular evolution of a magnetic field component perpendicular to the magnetic field loop [9].

4 Initial conditions

We choose the initial state of SF₆ gas in the shape of a circle. Compared with the circumambient air, the pressure and temperature of SF₆ within the circle is taken to be high. The detailed description of the parameters and their values can be seen from Table 1.

Table 1 Initial conditions of gases

Gas Species	Density(kg/m ³)	Pressure(Pa)	Temperature(K)	Molecular Weight
SF ₆	150.0	1.013×10 ⁷	1186.8	146
Air	1.205	1.013×10 ⁵	293.45	29

Meanwhile, the initial radius of SF₆ gas cloud $R_0 = 0.1$ m, the computational radial space of explosion is $15R_0$. The viscosity and thermal conduction are taken as 0.0000157 Pa.s and 0.0140676 W/(m·K), respectively. The magnetic field intensity is chosen to be 0.05T and its slope is equal to 1 (45°direction).

5 Results

Studies show that when the shock wave transmits from the heavy gas to the light gas, it produces a rarefaction wave propagating inward and induce RM instability to accelerate the interface mixing [10]. Both of the cold explosion of high pressure, high density SF₆ gas with and without magnetic field have been simulated.

5.1 Cold explosion without MHD

As shown in Fig.1. The traditional RM instability will experience four stages [10]: (1) Bifurcation stage of shock wave. At this stage, the incident shock wave interacts with interface and produces

transmitted shock wave and reflected wave.(2) Linear growth stage of instability (Fig.1.(b)). At this time, heavy fluids charge into light fluid and form spiky structures, while light fluid form bubble shaped structures for getting into heavy fluid. (3) Nonlinear growth stage of instability (Fig.1.(c)). Spiky structures narrow while the bubbles become wider, and the modification of spike structures are faster than the growth rate of bubble shaped structures.(4) Turbulent stage (Fig.1.(d) ~ Fig.1.(f)). At this stage, the secondary instabilities like KH instability will become more important. Spiky structures will be destroyed, then forms droplet shaped structure.

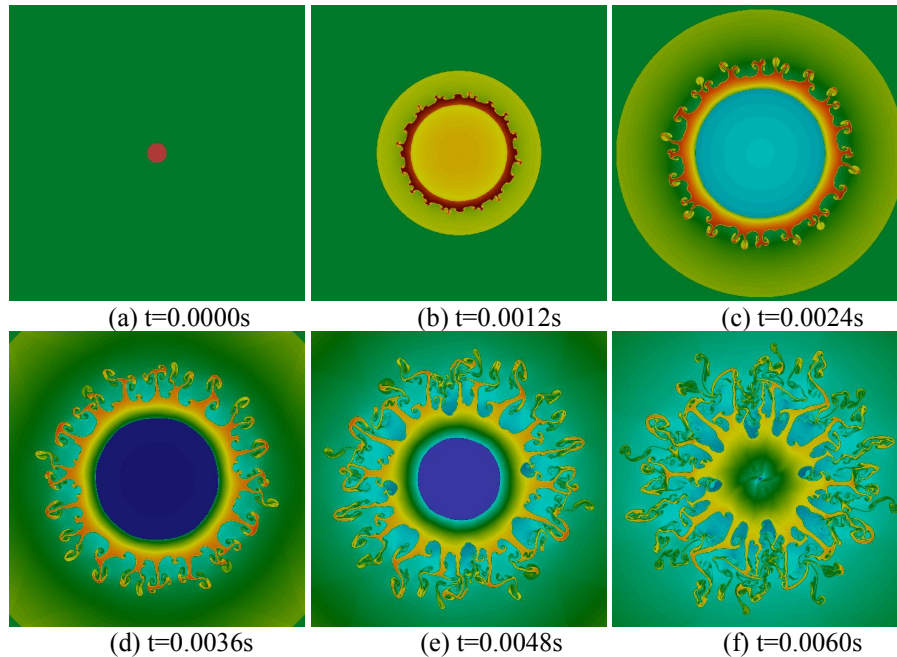


Fig.1. Evolution of the shock wave structure and flow interface of SF₆ gas cloud at different times.

Fig.2. depicts the propagation processes of reflected reshock at the center of circle. Initially, the strength of reflected shock wave is very high and the gas interface is ambiguous, most area of spiky heavy fluid and light “bubble” flow field become turbulent. Meanwhile, the reflected shock wave is propagating outward while turbulent gas is sucked inward (Fig.2.(a) ~ (b)), the interaction between them is very strong, which leads to the entire turbulence eventually (Fig.2.(c) ~ (d)).

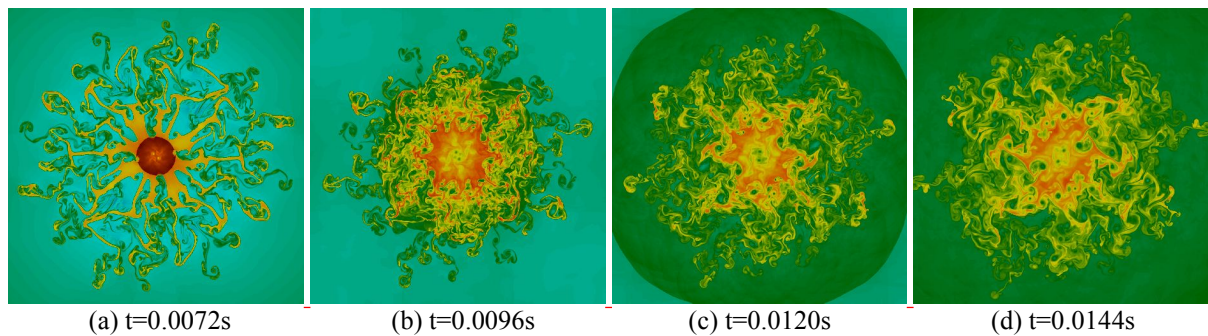


Fig.2. Processes of the interaction between reshock and the flow field.

5.2 Cold explosion with MHD

The applied magnetic field intensity is 0.05T and in the direction of northeast. Our numerical results are shown in Fig.3. To be more concisely, the time interval here is twice as much as its in Fig.1. It is clear that the basic processes are similar with Fig.1 and Fig.2. Instead of spiky and bubble shaped structure, there are more “droplets” and “mushrooms” in the flow field along the northeast direction

(45° direction), however, along the magnetic field direction, the interface are far more smoother. This phenomenon becomes more and more obvious over time. We conjecture that the magnetic field has the ability to prevent light fluid getting into heavy fluid to form “bubbles”, and it can prevent spiky structure from being crushed as well. To be more precisely, we study the magnetic energy term $\mathbf{B} \cdot \mathbf{B}/2\mu$ which also represents the influence of magnetic field on pressure intensity (eq.5).

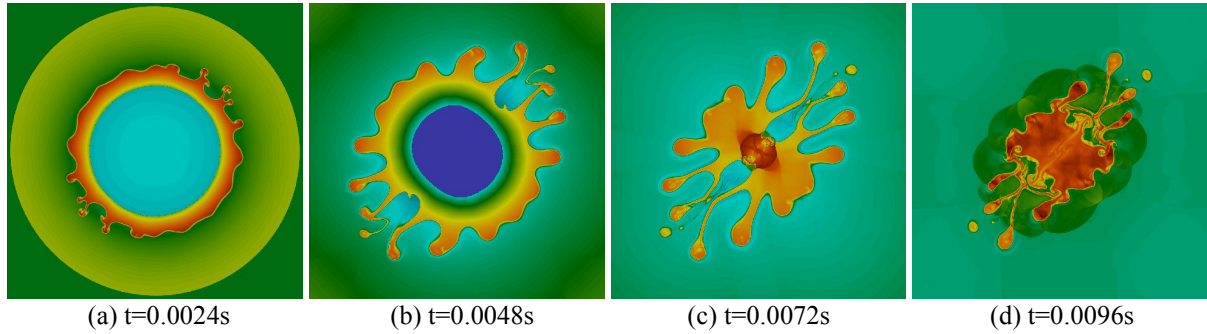


Fig.3. Evolution of the shock wave structure and flow interface when $B = 0.05T$.

Initially, the magnetic energy is equal in the whole flow field. Due to $\partial \mathbf{B}/\partial t - \nabla \times (\mathbf{v} \times \mathbf{B}) = 0$, \mathbf{B} changes faster where the partial derivatives of velocity is large, so that \mathbf{B} changes fast on the interface. At the beginning, the velocity difference on the interface is nearly the same because its density is homogeneous, also it is obvious that the movement parallel to the magnetic field is not affected by magnetic field force, thus, as we have observed, the magnetic energy on the interface becomes large and large quickly, especially on the position which is perpendicular to the initial magnetic field (\mathbf{B}_0). It prevents SF_6 and air protruding into each other on the interface as shown in Fig.4.(a) ~ (b). Gradually, the SF_6 gas cloud is squashed over time, then air and SF_6 begin to mix with each other and form bubble shaped structure along the direction which is perpendicular to the initial magnetic field, meanwhile, a few spikes show up where parallel to the \mathbf{B}_0 . At the same time, magnetic pressure imposes on the interface to prevent further instability. Fig.5 shows the magnetic induction lines which express the size and direction of the magnetic field at different times more clearly.

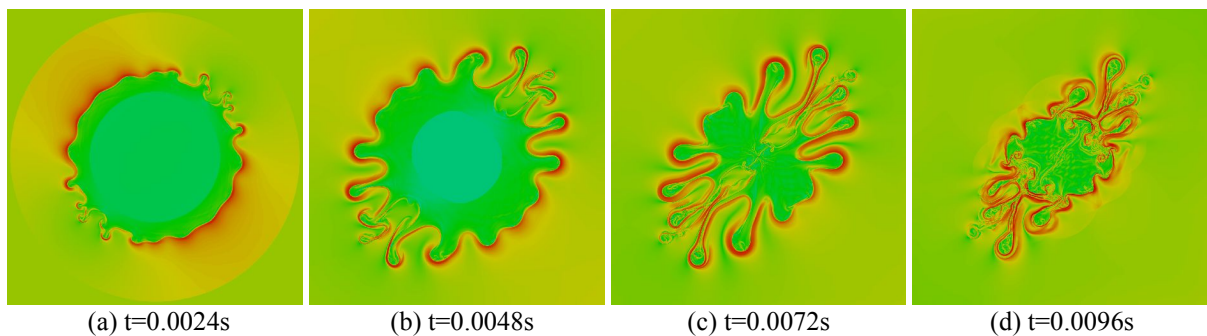


Fig.4. Magnetic energy contours in the flow field at different times.

Fig.6 illustrates the pressure distributions along the radius at different times. Initially, SF_6 gas cloud expands sharply due to the influence of internal high pressure, then the transmitted shock wave and reflected rarefaction wave are formed through gas interface, the transmitted shock wave propagates outward under the high pressure. With the propagating of transmitted shock wave, the pressure of wave front attenuates quickly whereas the speed of transmitted shock wave is very fast. Now take a look at rarefaction wave, its pressure is far lower than the pressure of transmitted shock wave. At the beginning of the formation, rarefaction wave spreads outward along with gas interface which moves supersonically, and the pressure of rarefaction wave decreases gradually.

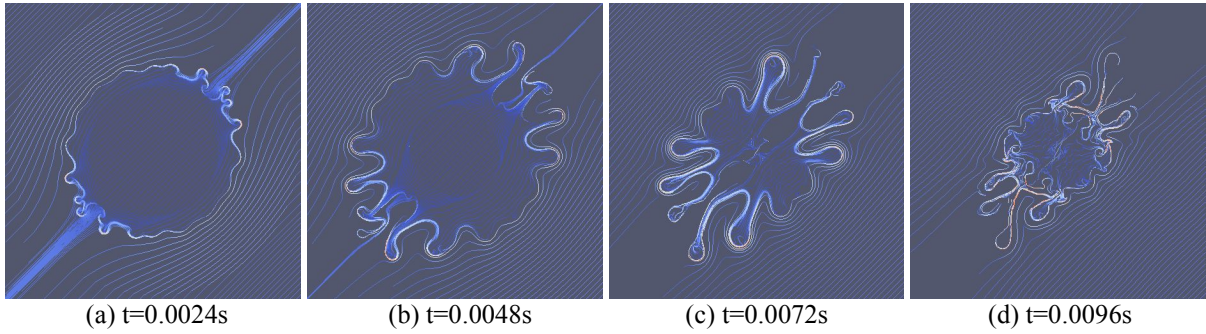


Fig.5. Magnetic induction line in the flow field at different times.

On the other hand with the rapid expansion of SF₆ gas cloud, the pressure in center of the circle becomes extremely low, whereafter, the rarefaction wave propagates inward leading to convergence in the center of sphere and then form the reshock. Once the rarefaction wave converges, the pressure at the center and suddenly leads to the maximum pressure of about 320kPa. Meanwhile, the reshock moves outward quickly, and interact with the original interface and accelerate the turbulent transition in the flow field, the pressure in the area where secondary shock wave has traveled through fluctuates, the pressure of reshock front decreases rapidly at the same time. As shown in Fig.6.(b), there are some protrusions on the interface which indicate the influence of magnetic field. Meanwhile, the reshock recedes more quickly.

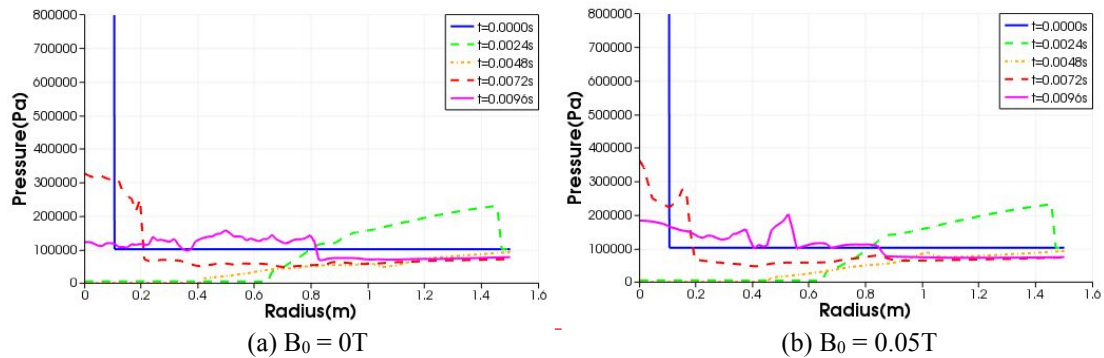


Fig.6. Pressure distributions along the radius at different times. (The right figure with $B_0 = 0.05T$)

In order to see the influence of magnetic field more clearly, Fig.7. show the magnetic energy along the radius at different times. At first, With the propagating of transmitted shock waves, the interface moves outward, so is the region where magnetic energy gathers. As time goes by, air and SF₆ charge into each other so that the shape of interface is irregular. The region where has the maximum of magnetic energy moves back. After the rarefaction waves converge at the center and form reshock, the whole flow field begins to appear turbulent state, meanwhile, the major area which is influenced by magnetic force moves inward. At last, the magnetic field still has impact on the flow field, the region where is influenced by the magnetic field most is between 0.4m and 0.6m along the radius at that moment.

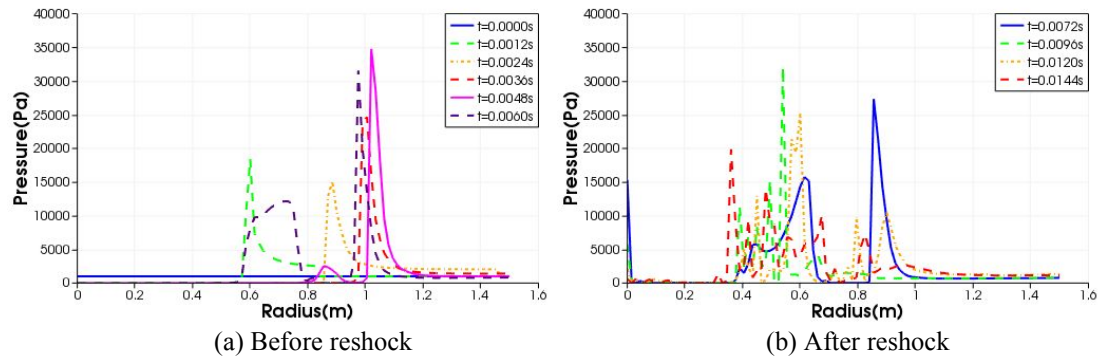


Fig.7. Magnetic energy distribution along the radius at different times (due to eq.5, they have the same units with pressure)

With the adding of proper magnetic field, RM instability can be controlled effectively, especially on the interface which is perpendicular to the initial magnetic field. The whole high density gas cloud will be squashed over time. At last, when the whole flow field becomes fully turbulent state, the fluid micelle appears bubble shaped structure because of continuous effect of magnetic field.

References

- [1] Holmes, R. L., Grove, J. W., and Sharp, D. H. Numerical investigation of Richtmyer-Meshkov instability using front-tracking. *J. Fluid Mesh.*, 301, 51-64(1995)
- [2] Chern, I.-L., Glimm, J., McBryan, O., Plohr, B., and Yaniv, S. Front tracking for gas dynamics. *J. Comput. Phys.*, 62, 83-110(1986)
- [3] Glimm, J., Li, X. L., Liu, Y. J., Xu, Z. L., and Zhao, N. Conservative front-tracking with improved accuracy. *SIAM J. Numer. Anal.*, 41(5), 1926-1947(2003)
- [4] Glimm, J., Graham, M. J., Grove, J., Li, X. L., Smith, T. M., Tan, D., Tangerman, F., and Zhang, Q. Front tracking in two and three dimensions. *Comput. Math. Appl.*, 35, 1-11(1998)
- [5] Holmes, R. L., Dimonte, G., Fryxell, B., Gittings, M. L., Grove, J. W., Schneider, M., Sharp, D. H., Velikovich, A. L., Weaver, R. P., and Zhang, Q. Richtmyer-Meshkov instability growth: experiment, simulation and theory. *J. Fluid Mech.*, 389, 55-79(1999)
- [6] Howell, B. P. And Ball, G. J. Damping of mesh-induced errors in free-Lagrange simulations of Richtmyer-Meshkov instability. *Shock Waves*, 10, 253-264(2000)
- [7] Li, X. L. and Zhang, Q. A comparative numerical study of the Richtmyer-Meshkov instability with nonlinear analysis in two and three dimensions. *Phys. Fluids*, 9, 3069-3077(1997)
- [8] Saltzman J. An unsplit 3D upwind method for hyperbolic conservation laws, *J. Comput. Phys.* 115 (1994) 153.
- [9] Gardiner T.A., Stone J. M. An unsplit Godunov method for ideal MHD via constrained transport, *J. Comput. Phys.* 205 (2005) 509.
- [10] Zhuang, Z. H., Xue, D. W., Chen, Z. H., Jiang, X. H. The eruption of a high-pressure cylindrical heavy gas cloud. *Canadian Journal of Physics*, 2013, 91:850-854